J Neuropathol Exp Neurol

Vol. 66, No. 4
April 2007
pp. 272–283

ORIGINAL ARTICLE

Nitric Oxide Synthase 3-Mediated Neurodegeneration After Intracerebral Gene Delivery

Suzanne M. de la Monte, MD, MPH, Ami Jhaveri, AB, Bradley A. Maron, MD, and Jack R. Wands, MD

Abstract

In Alzheimer disease (AD), increased nitric oxide synthase 3 (NOS3) expression correlates with apoptosis in cortical neurons and colocalizes with amyloid precursor protein (APP)-amyloid β (Aβ) deposits in the brain. In the present study we examined the potential role of NOS3 in relation to AD-type neurodegeneration using an in vivo model of gene delivery. Long Evans rat pups were given a single intracerebral injection of recombinant plasmid DNA containing the human NOS3 cDNA (p-hNOS3) or the luciferase (p-Luc) gene as a negative control, and complexed with polyamine reagent. Overexpression of NOS3 in the brain increased the levels of APP, APP-Aβ, p53, Tau, glial fibrillary acidic protein, and peroxisome proliferator activated receptors (PPAR) δ and γ and decreased the levels of Hu (neuronal marker) mRNA, phosphorylated glycogen synthase kinase 3β, ATP synthase, and choline acetyltransferase expression as demonstrated by real-time quantitative reverse-transcribed polymerase chain reaction, Western blot analysis, or immunohistochemical staining. These effects of NOS3 overexpression were accompanied by increased single-stranded DNA immunoreactivity, reflecting DNA damage. The results suggest that increased cerebral expression of NOS3 causes several molecular abnormalities related to AD-type neurodegeneration, including oxidative stress, mitochondrial dysfunction, and impaired acetylcholine homeostasis. The coexisting increases in PPAR-δ and -γ expression suggest that the adverse effects of NOS3 overexpression may be abated by PPAR agonist treatment.

Key Words: Experimental model of neurodegeneration, In vivo gene delivery, Nitric oxide synthase.

INTRODUCTION

Nitric oxide (NO) is a free radical gas that functions as a diffusable neurotransmitter and inter- and intracellular signaling molecule in the brain (1). At low concentrations, NO reversibly inhibits cytochrome oxidase in competition with oxygen and may have an important role in the physiologic regulation of cellular energy metabolism. At high concentrations, other respiratory chain complexes can be inhibited by nitrosylation of critical tyrosine residues or oxidation of protein thiols and removal of iron from the iron-sulfur centers. Very high concentrations of NO promote the generation of peroxynitrite anion ($ONOO^-$), a reaction product of superoxide plus NO, which causes irreversible inhibition of mitochondrial respiration and damage to various mitochondrial components via oxidizing reactions. Therefore, NO and its derivative peroxynitrite, inhibit mitochondrial respiration by distinct mechanisms. In addition to the direct effects of NO on cell function, many NO-associated physiologic actions are mediated through increased cGMP synthesis by soluble guanylate cyclase, leading to activation of signaling cascades involving cGMP-dependent protein kinase (2, 3).

Nitric oxide synthases (NOSs) generate NO through oxidation of the guanidino nitrogen of L-arginine. NOS1 and NOS3, initially identified in neurons and endothelial cells, respectively, are stimulated to synthesize NO by calcium/calmodulin signaling (3, 4). Expression of the NOS2 isoform has been detected in a number of cell types and typically is induced by lipopolysaccharide or proinflammatory cytokine stimulation (5–7). In addition, the existence of a fourth NOS isoform, mitochondrial NOS, and its Ca^{2+} dependence and relevance for mitochondrial bioenergetics were reported (8–10). In disease states such as inflammation, infection, ischemia, excitotoxic injury, or neurodegeneration, the expression levels of one or more NOS isoforms may be increased. Elevated levels of NOS expression and NO synthesis can be either detrimental or essential to cell viability and function. For example, experimental treatment of cultured neurons with NO donors can cause growth cone collapse (11), and, in vivo, high levels of NOS expression can inhibit postinjury neuronal regeneration (12). These adverse effects of NO can be blocked by inhibiting NOS enzyme activity or gene expression (12–14), enhancing superoxide dismutase activity (15), treating cells with free radical/peroxynitrite scavengers (3), providing suitable growth factors after injury (4, 16), repleting cofactors that favor NO signaling rather than free radical generation, or genetically depleting NOS (5, 17). However, in some neurons, NO plays a key role in synaptic plasticity, long-term potentiation (18), neurite outgrowth (16, 17), and basal functions (8, 13), indicating that abolishment of NOS gene expression or NOS enzyme activity, even in disease states,

From the Departments of Medicine and Pathology and Division of Neuropathology, Rhode Island Hospital, Brown Medical School, Providence, Rhode Island.
Send correspondence and reprint requests to: Dr. S. M. de la Monte, Rhode Island Hospital, Brown Medical School, 55 Claverick Street, Room 419, Providence, RI 02903; E-mail: Suzanne_DeLaMonte_MD@Brown.edu
This work was supported by COBRE Grant P20RR15578 and Grants AA02666, AA02169, AA11431, and AA12908 from the National Institutes of Health.
A supplementary figure is available online at http://www.jneuropath.com.

would not benefit all neurons and most likely would have harmful effects in the brain.

Dementia in Alzheimer disease (AD) is correlated with cell loss and synaptic disconnection (19) mediated by apoptosis, increased mitochondrial DNA damage, impaired mitochondrial function, and constitutive activation of pro-apoptotic mechanisms (20–30). Previous studies linked AD neurodegeneration to elevated levels of NOS2 and NOS3 expression in degenerating cortical neurons (31–34). Although the high levels of NOS2 observed in neurons with neurofibrillary tangles suggest a role for proinflammatory cytokine activation in association with neuronal loss in AD (34), the more abundant and widely distributed abnormalities in NOS3 expression, combined with its early onset of aberrant gene expression in relation to the time course of cognitive impairment (31–33), suggest that the NOS3 isoform has a pivotal role in the AD neurodegeneration cascade.

The mechanism by which NOS3 overexpression contributes to neuronal loss was partially elucidated from in vitro studies in which human central nervous system-derived neuronal cells were infected with recombinant adenovirus carrying the NOS3 cDNA (35). Those studies demonstrated that NOS3 overexpression results in apoptosis and mitochondrial dysfunction accompanied by increased levels of proapoptosis molecules, including p53, p21/Waf1, Bax, and CD95. In that context, mitochondrial dysfunction was associated with increased oxidative stress, plasma membrane leakiness, mitochondrial permeability transition, and enhanced sensitivity to reactive oxygen species (35). To extend our evaluation of NOS3-mediated neurodegeneration, we used recombinant plasmid DNA-based gene delivery to overexpress NOS3 in the brain. The objective was to determine the degree to which NOS3 overexpression causes molecular and biochemical lesions associated with AD-type neurodegeneration in vivo.

MATERIALS AND METHODS

Gene Delivery Model

Eight-day-old Long Evans rats were anesthetized with pentobarbital (40 mg/kg) and given intraventricular/intracerebral injections of recombinant plasmid DNA containing the complete coding sequence of human NOS3 (p-hNOS3) (31) or luciferase (p-Luc) as a negative control. The cDNAs were ligated into the pcDNA3.1 vector (Invitrogen, Carlsbad, CA) in which gene expression was under the control of a cytomegalovirus promoter. Super-coiled plasmid DNA was purified using endotoxin-free columns (QIAGEN, Inc., Valencia, CA). For each animal, 10 μg of recombinant plasmid DNA were complexed with 10 μL of the Mirus Transit In Vivo polyamine reagent (Panvera, Inc., Madison, WI), and then mixed with 10 μL of 10× Transit In Vivo diluent plus 20 μL of sterile water. DNA-polymer solution (25 μL) was injected into the right lateral ventricle over a period of 5 minutes using a Hamilton syringe with a 26-gauge needle fixed in a stereotaxic frame. All animals survived the procedure and exhibited normal behavior within 10 minutes of awakening from anesthesia. There were no subsequent deaths, aberrant behaviors, or adverse responses such as failure to thrive, poor grooming, reduced physical activity, or weight loss. Rats were killed 1 to 7, 14. or 30 days after DNA inoculation to detect histopathologic lesions and assess changes in gene expression. Eight-day-old rats were used in this study because at that age the rat cerebrum is relatively well developed, the animals easily tolerated the injections, and central nervous system plasmid-based gene delivery could be achieved consistently. In contrast, exploratory studies demonstrated relatively poor plasmid-based gene delivery and expression in the adult rat brain. The procedures and use of rats in experiments were approved by

TABLE. Primer Pairs Used to Measure mRNA Levels by Real-Time Quantitative Reverse-Transcribed Polymerase Chain Reaction

Gene	Forward Primer Sequence (5′→3′)	Reverse Primer Sequence (5′→3′)	Amplicon (bp)
18S	GGA CAC GGA CAG GAT TGA CA	ACC CAC GGA ATC GAG AAA GA	50
hNOS3	AGA TGA GCC CCC AGA ACT CTT C	TGG TCC ACG ATG GTG ACT TTG	371
rNOS1	CCA GTC TTC CTG ACC TGT TGC TTA G	TCA TCT GCT CAT TCC GAT TCG	149
rNOS2	AAG AGG AAC AAC TAC TGC TGG TGG	CCA AAT ACC GCA TAC CTG AAG G	133
rNOS3	CGC AAA AGG AAG GAA TCC AGT AAC	CCC AAA CAC ACA GAA CCT GAG G	72
APP	TGC CAAC CAC TAC CAC AAC TA	GTT CTG CAT CTG CTC AAA G	1,464
COX4	GAG AGC CAT TTC TAC TTC GGT GTG	CCA CTC ATT GGT GCC CTT GTT C	265
ATP Syn	AGA CTG GTT TTG GAG GTA GCC C	ATT TTG ATT GGT GCC CCC G	122
UCP2	TGT TCT CCT GTG TAT TCT CCT GCG	AAG GTG TCC CGT TCT TCA AAG C	138
UCP4	TGG TCA CCT ACG AAC ATC TCC G	TGG GGT TGG CTA AAA ACT GTC C	126
UCP5	TGA TAG TTT CAG GAA TGC TGG GAG	AGT TCT CAC CAC ATC CAC AGG G	110
PPAR-α	TAC TGC CGT TTC CAC AAG TGC C	TTC ATC AAG GAG GAC AGC ATC G	514
PPAR-γ	AAG ACG GAT TGC CCT CAT TTG ATG	TGT TGC GAC TGC GGT TGT GTA	441
PPAR-δ	CCA GAA GAA CCG CAA CAA G	TCG TGG ATG ATG AAG GGT GC	293

Primer sequences used to measure mRNA levels of human (h) nitric oxide synthase 3 (NOS3), rat (r) NOS1, rNOS2, and rNOS3, amyloid precursor protein 770 (APP), mitochondrial cytochrome oxidase, subunit 4 (COX4), mitochondrial ATP synthase (Syn), uncoupling protein (UCP) 2, UCP4, and UCP5, and peroxisome proliferator-activated receptor (PPAR) subtypes α, γ, and δ. The nucleic acid sequences of the primers used to measure 18S ribosomal RNA levels, for normalizing results and thereby enabling intergroup comparisons, are also provided. The amplicon sizes are indicated in Column 4. In each instance, gel electrophoresis studies demonstrated amplification of a single product generated with the indicated primer pairs, and the amplicon was verified by nucleic acid sequencing.

the Lifespan-Rhode Island Hospital institutional animal care and use committee.

Tissue Studies

Upon death, the brains were harvested and either immersion fixed in Histochoice fixative (Amresco Corp., Solon, OH) for paraffin embedding or sliced fresh to microdissect the temporal lobe. Fresh tissue was snap-frozen in a dry ice-methanol bath and stored at −80°C for mRNA and protein studies. For histopathologic and immunohistochemical studies, the fixed brains were sectioned in the coronal plane and embedded in paraffin. Histologic sections (8 μm thick) stained with hematoxylin and eosin were subjected to image analysis to measure the cross-sectional area of the right temporal lobe and cell density within the

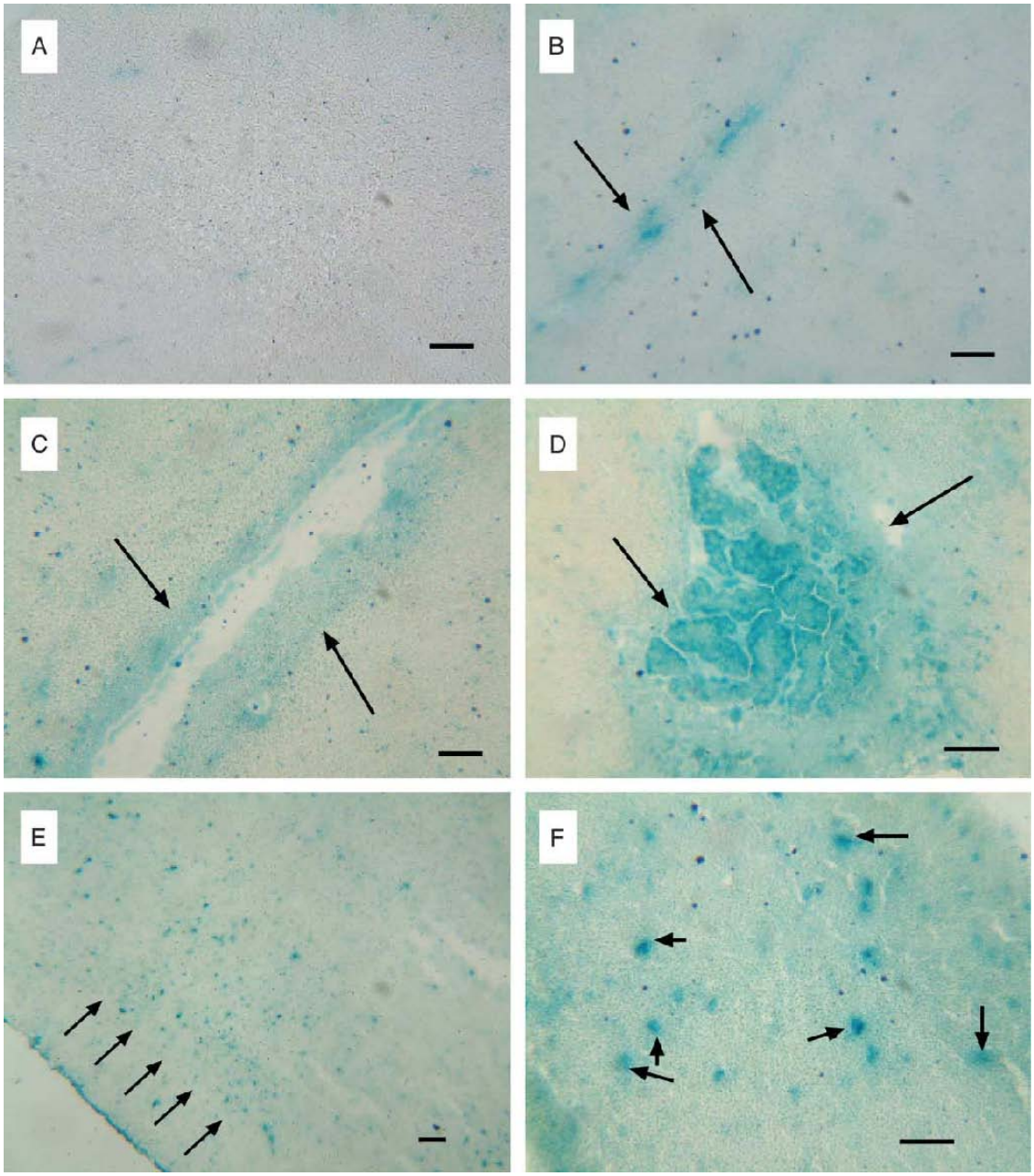

FIGURE 1. *LacZ* expression detected in brain tissue by enzyme histochemistry. Rat pups were given a single intraventricular/intracerebral injection of recombinant plasmid DNA expressing luciferase (p-Luc) **(A)** or LacZ **(B–F)** using polyamine reagent. Brains harvested 14 days later from the p-Luc-inoculated control **(A)**, and pLacZ-inoculated experimental **(B–F)** groups were analyzed for β-galactosidase activity (blue precipitate). Arrows point to leptomeninges **(B)**, ependymal cells **(C)**, choroid plexus **(D)**, and cortical cells **(E, F)**. (**F**) Higher magnification image demonstrates labeling of various cell types within the cortex and white matter. Scale bars = 25 μm.

right temporal cortex at the level of the infundibulum. The measurements were made using ImagePro Plus software (Media Cybernetics, Inc., Silver Spring, MD). Size, shape, and color parameters for nuclei were preset, and the cell counting was automated with manual correction of computer errors. The slides were coded, and measurements were made by a coinvestigator who was naive to the experimental design. Adjacent paraffin sections were immunostained with antibodies to NOS3, glial fibrillary acidic protein (GFAP), proapoptosis genes (p53 and Bax), and amyloid precursor protein (APP)-amyloid β (Aβ). Immunoreactivity was detected with biotinylated secondary antibody, horseradish peroxidase-conjugated avidin-biotin complexes, and either NovaRed or diaminobenzidine (Vector Laboratories, Burlingame, CA) as the chromogen (22, 31).

Quantitative mRNA Studies

mRNA expression levels were evaluated using quantitative real-time reverse-transcribed (RT) polymerase chain reaction (PCR) assays. Total RNA was isolated from the right temporal cortex using TRIzol reagent (Invitrogen) according to the manufacturer's protocol. Samples containing 2 μg of RNA were reverse-transcribed with the AMV First Strand cDNA synthesis kit (Roche Diagnostics, North America, Indianapolis, IN) and random oligodeoxynucleotide primers. PCR assays were used to measure mRNA levels of hNOS3, rat (r) NOS1, rNOS2, rNOS3, Hu (neuron), myelin-associated glycoprotein 1, APP, mitochondrial cytochrome oxidase, subunit IV (COX), ATP synthase, uncoupling protein (UCP) 2, UCP4, and UCP5, peroxisome-proliferator activated receptors (PPAR) α, δ, and γ, choline acetyltransferase, and acetylcholinesterase.

PCR primer pairs were designed using MacVector 8.1 software (Accelrys, Inc., Oxford Molecular Ltd., Oxford, UK). Ribosomal 18S RNA levels measured in parallel reactions were used to calculate the relative abundance of each mRNA transcript (36, 37). Ribosomal 28S RNA levels were also measured, and the corresponding 28S/18S ratios were calculated to further assess RNA integrity. PCR amplifications were performed in 25-μL reactions containing cDNA generated from 2.5 ng of original RNA template, 300 nmol/L each of gene-specific forward and reverse primers (Table), and 12.5 μL of 2× QuantiTect SYBR Green PCR Mix (QIAGEN, Inc.). The amplified signals

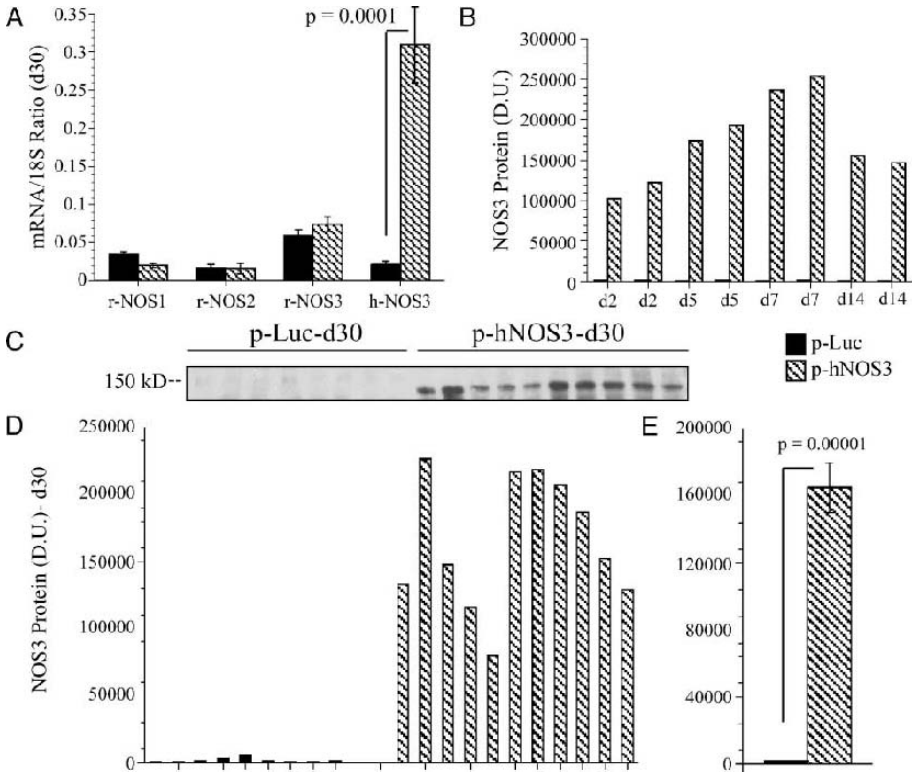

FIGURE 2. Cerebral nitric oxide synthase (NOS) expression after recombinant plasmid-based gene delivery. Rat pups were given a single intraventricular/intracerebral injection of recombinant plasmid DNA expressing p-Luc or p-hNOS3 using polyamine reagent. **(A)** Brains harvested up to 30 days later to measure relative levels (mean ± SD) of endogenously expressed rat (r) NOS1, rNOS2, and rNOS3, and transfected human NOS3 mRNA by real-time quantitative reverse-transcribed polymerase chain reaction. Results were normalized to 18S rRNA (n = 8 samples/group). **(B)** Time course analysis of NOS3 protein expression in brains harvested 2, 5, 7, or 14 days (d) after gene delivery. NOS3 expression was detected by Western blot analysis and quantified by digital imaging in densitometry units (D.U.). Each bar corresponds to an individual brain. **(C, D)** Cerebral NOS3 protein expression 30 days after gene delivery as demonstrated by Western blot analysis **(C)** and digital image quantification **(D)**. **(E)** Mean ± SD levels of NOS3 protein measured in control and p-hNOS3-inoculated rat brains. Intergroup statistical comparison was made using the Student *t*-test.

were detected continuously with the Bio-Rad iCycler iQ Multi-Color RealTime PCR Detection System (Bio-Rad, Hercules, CA). The amplification protocol used was as follows: initial 15-minute denaturation and enzyme activation at 95°C, 45 cycles of 95°C × 15 seconds, 55 to 60°C × 30 seconds, and 72°C × 30 seconds. Annealing temperatures were optimized using the temperature gradient program provided with the iCycler software.

In preliminary studies, SYBR Green-labeled PCR products were evaluated by agarose gel electrophoresis, and the authenticity of each amplicon was verified by nucleic acid sequencing. The cDNAs were cloned into PCRII vector (Invitrogen). Serial dilutions of known quantities of recombinant plasmid DNA containing the specific target sequences were used as standards in the PCR reactions, and the regression lines generated from the C_t values of the standards were used to calculate mRNA abundance. To correct for differences in template loading, the ng ratios of specific mRNA to 18S were calculated (36, 37), thereby providing indices of relative transcript abundance, which were used to make intergroup comparisons. Results were normalized to 18S because 18S is highly abundant, and the levels were essentially invariant among the samples, whereas housekeeping genes were frequently modulated by the disease state. Intergroup statistical comparisons were made using the calculated mRNA/18S ratios. Negative control studies included real-time quantitative PCR analysis of 1) template-free reactions; 2) RNA that had not been reverse-transcribed; 3) RNA samples that were pretreated with DNase I; 4) samples treated with RNase A before the reverse transcriptase reaction; and 5) genomic DNA.

Western Blot Analysis

Tissue samples were homogenized in 5 volumes of radioimmunoprecipitation assay buffer (50 mmol/L Tris-HCl, pH 7.5, 1% Nonidet P-40, 0.25% sodium deoxycholate, 150 mmol/L NaCl, 1 mmol/L EDTA, and 2 mmol/L EGTA) containing protease (1 mmol/L phenylmethylsulfonyl fluoride, 0.1 mmol/L *N*-tosyl-l-phenylalanine chloromethyl ketone, 1 μg/mL aprotinin, 1 μg/mL pepstatin A, 0.5 μg/mL leupeptin, 1 mmol/L NaF, and 1 mmol/L $Na_4P_2O_7$) and phosphatase (2 mmol/L Na_3VO_4) inhibitors. Cellular debris was pelleted by centrifuging the samples at 14,000 × *g* for 15 minutes at 4°C, and supernatant fractions were used in the studies. Protein concentrations were determined using the bicinchoninic acid assay (Pierce Chemical, Rockford, IL). Aliquots containing 60 or 100 μg of protein were fractionated by sodium dodecyl sulfate-polyacrylamide gel electrophoresis using the Bio-Rad 16-cm Vertical Electrophoresis Apparatus (Bio-Rad) (38). Although 25 or 50 μg of protein can be analyzed by Western blotting, for our studies we used larger amounts to increase the signal-to-noise ratio and detect lower amounts of the proteins of interest in control temporal lobe samples. Proteins were transferred to polyvinylidene difluoride membranes, and nonspecific binding sites were adsorbed with SuperBlock-TBS (Pierce Chemical). The membranes were then incubated overnight at 4°C with primary antibody (0.5–1 μg/mL) diluted in Tris-buffered saline (50 mmol/L Tris and 150 mmol/L NaCl, pH 7.4) containing 1% bovine serum albumin and 0.05% Tween-20. Immunoreactivity was detected with horseradish peroxidase-conjugated secondary antibody and enhanced chemiluminescence reagents, and quantified by digital imaging with the Kodak Digital Science Imaging Station (DuPont-NEN Life Sciences Products, Inc., Boston, MA).

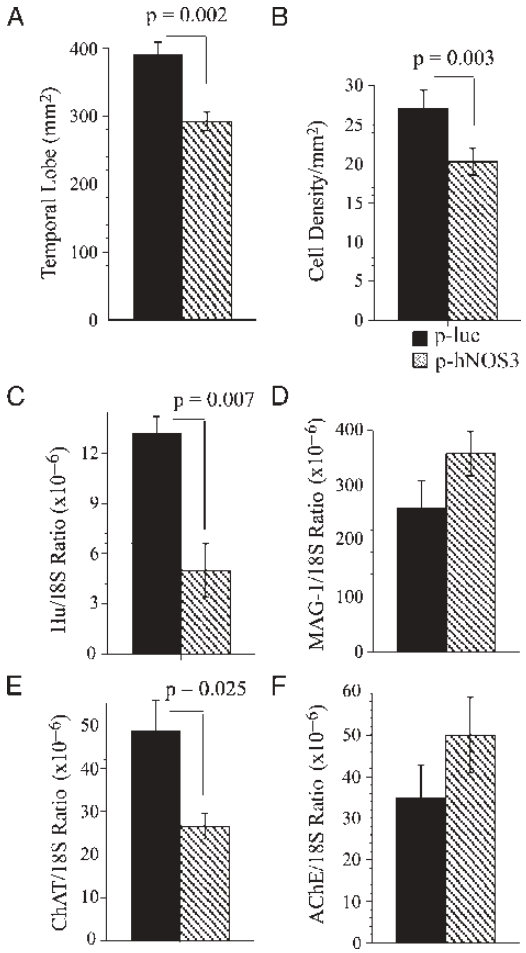

FIGURE 3. Cerebral atrophy and neuronal loss with increased NOS3 expression in the temporal lobe. Brains from pups inoculated with p-Luc or p-hNOS3 were harvested 30 days after gene delivery. Histologic sections made at the level of the infundibulum were stained with hematoxylin and eosin and subjected to image analysis to measure the cross-sectional area (mm^2) **(A)** and cell density (per mm^2) in the temporal cortex **(B)** using Image-Maker Pro 3 software. Twelve samples were analyzed per group. Total RNA was extracted from temporal lobe homogenates (infundibulum level) and reverse-transcribed, and the resulting cDNAs were used for real-time quantitative reverse-transcribed polymerase chain reaction to measure the mRNA levels of **(C)** Hu, **(D)** myelin-associated glycoprotein-1 (MAG-1), **(E)** choline acetyltransferase (ChAT), and **(F)** acetylcholinesterase (AChE) (see Materials and Methods section). The ng quantities of mRNA were normalized to 18S rRNA measured in the same samples. The group means ± SEM corresponding to the relative levels of gene expression are depicted graphically. Intergroup differences were evaluated using Student *t*-tests and significant p values are indicated over the bars.

Source of Reagents

Monoclonal antibodies to p53 and β-actin were obtained from Oncogene Research Products (Cambridge, MA), and monoclonal antibodies to NOS3 were purchased from Transduction Laboratories (Lexington, KY). Polyclonal antibodies to Bax and GFAP were purchased from Santa Cruz Biotechnology (Santa Cruz, CA). Monoclonal antibodies to APP, APP-Aβ, and Tau were purchased from Calbiochem-Novabiochem (La Jolla, CA). Biotinylated secondary antibody and the ABC Elite kit used to perform immunohistochemical staining were purchased from Vector Laboratories. Oligodeoxynucleotide primers were commercially synthesized (Invitrogen).

Statistical Analysis

Graphs depict the means ± standard errors of the means of results from up to 20 rats per group. Intergroup comparisons were made using Student *t*-tests. Data analysis was performed using the Number Cruncher Statistical System (Version 2002; Dr. Jerry L. Hintze, Kaysville, UT).

RESULTS

Time Course and Distribution of Gene Expression

In preliminary experiments, intracerebral/intraventricular gene delivery was performed using recombinant plasmid DNA expressing the *LacZ* gene, and β-galactosidase activity was detected by enzyme histochemistry. Although the DNA was inoculated into the right cerebral hemisphere and lateral ventricle, and increased β-galactosidase activity was initially (first 2 days) detected ipsilateral to the injection, over time (7–14 days post-inoculation), increased β-galactosidase was detected at similar levels in both cerebral hemispheres. Expression of the foreign gene was first detected in the choroid plexus and ependymal cells (24–48 hours), followed by leptomeningeal

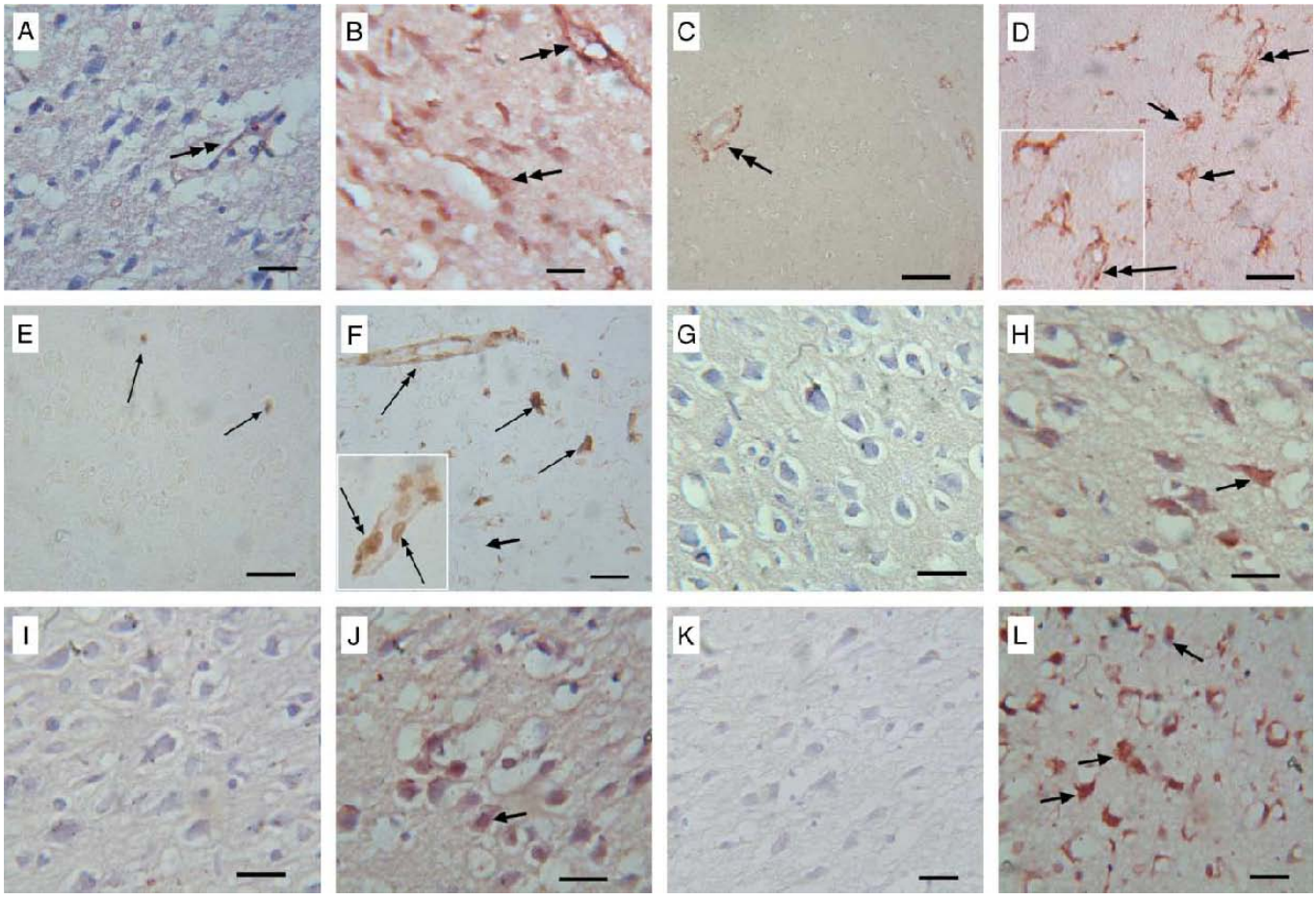

FIGURE 4. Effects of NOS3 overexpression on tissue injury, proapoptosis gene expression, and amyloid precursor protein-amyloid β (APP-Aβ) immunoreactivity. Brains from pups inoculated with p-Luc **(A, C, E, G, I, K)** or p-hNOS3 **(B, D, F, H, J,** and **L)** were harvested 30 days after gene delivery. Adjacent histologic sections of brain were immunostained to detect NOS3 **(A, B)**, glial fibrillary acidic protein **(C, D)**, single-stranded DNA **(E, F)**, Bax **(G, H)**, p53 **(I, J)**, or APP-Aβ **(K, L)**. Immunoreactivity was revealed using the ABC method with diaminobenzidine as the chromogen. Representative staining patterns in the temporal cortex (infundibulum level) are depicted. Single-headed arrows indicate labeled parenchymal cells; double-headed arrows indicate labeled microvessels. Scale bars = 25 μm.

vessels (48–72 hours) and then the intracerebral microvasculature (48–96 hours). Between 4 and 7 days after gene delivery, expression of the transgene persisted in the leptomeninges, choroid plexus, and ependymal lining cells, and gradually increased in various cell types distributed in both gray and white matter structures (Fig. 1). The peak levels of β-galactosidase activity occurred by day 14. Thereafter, the levels gradually declined, although at the 30-day point, the levels were still elevated above control. This time line was used to investigate the effects of NOS3 overexpression in the brain.

Human NOS3 mRNA and Protein Expression After Intracerebral Gene Delivery

The real-time quantitative RT-PCR studies demonstrated increased levels of hNOS3 mRNA within 48 hours of gene delivery and persistently elevated levels of hNOS3 up to 30 days after injection of DNA. At the 30-day time point, significantly increased mean levels of hNOS3 mRNA were measured in brains injected with p-hNOS3 relative to the p-Luc-inoculated control brains ($p = 0.0001$) (Fig. 2A). In contrast, rNOS1, rNOS2, and rNOS3 mRNA transcripts were similarly abundant in both groups (Fig. 2A). Western blot analysis demonstrated progressively increased levels of NOS3 expression during the first 7 days after p-hNOS3 inoculation, and slightly lower levels of NOS3 protein expression by day 14 (Fig. 2B). Although the NOS3 antibody cross-reacted with endogenously expressed rNOS3, the relatively low levels of NOS3 detected in control brains indicate that the contributions of endogenously expressed NOS3 to the Western blot signals were minimal. Western blot analysis demonstrated the expected ~135 kDa band corresponding to NOS3 and prominently elevated levels of NOS3 30 days after p-hNOS3 gene delivery (Fig. 2C). Digital imaging of the Western blot signals revealed uniformly low levels of NOS3 in p-Luc-transfected control brains, and high levels of NOS3 in brains inoculated with p-hNOS3 (Fig. 2D). Statistical analysis demonstrated significantly higher mean levels of NOS3 protein in brains inoculated with p-hNOS3 relative to those inoculated with p-Luc ($p = 0.00001$) (Fig. 2E).

Brain Tissue Studies

The histologic studies were focused on brains harvested 30 days after gene delivery. We used two independent approaches to estimate the extent and nature of NOS3-mediated neurodegeneration: two-dimensional morphometric analysis and molecular profiling of brain cell type-specific genes. The latter approach was developed to provide an objective, quantitative, and relatively rapid means of evaluating relative cell loss with neurodegeneration and was successfully used to characterize neurodegeneration in human cases and experimental animal models of AD (39–41). Image analysis of hematoxylin and eosin-stained sections demonstrated that the mean cross-sectional area and mean cell density (counting nuclei) were

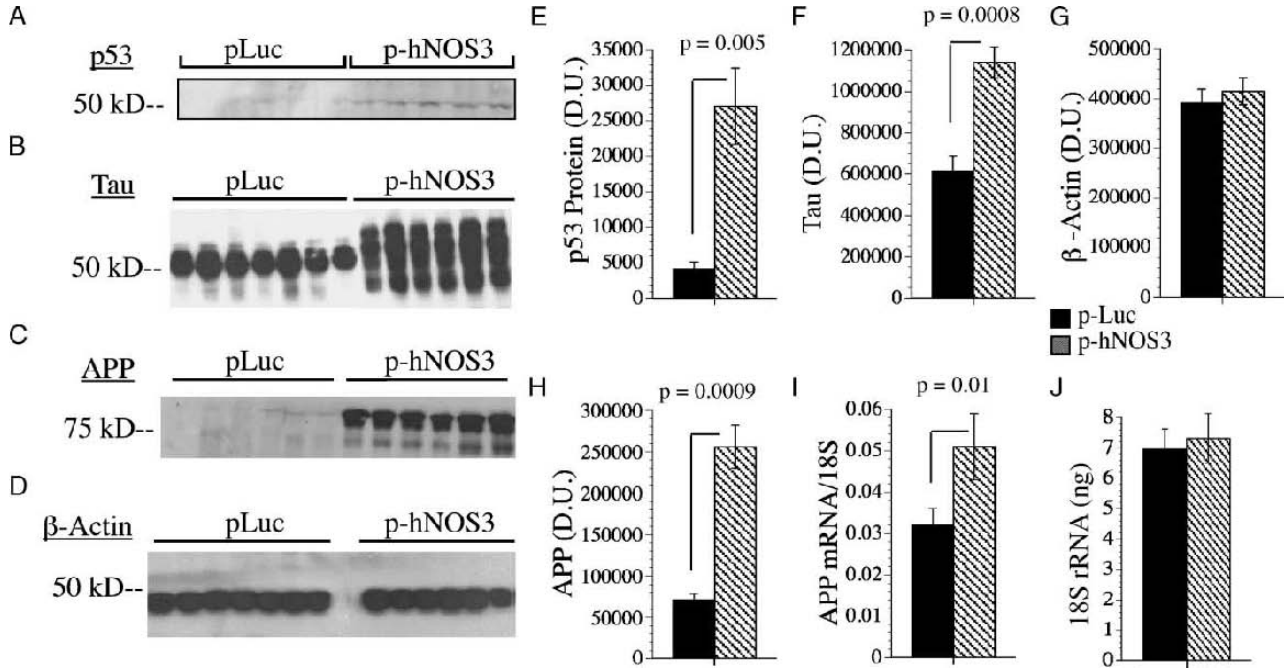

FIGURE 5. Increased proapoptosis and AD-associated proteins with NOS3 overexpression in brain. Temporal cortex tissue from p-Luc- or p-hNOS3-inoculated rats (day 30) was subjected to Western blot analysis to measure levels of p53 **(A)**, Tau **(B)**, APP **(C)**, or β-actin **(D)**. Molecular weight standards were included in all blots, and the position of the ~50 or ~75 kDa marker is shown at the left. Immunoreactivity corresponding to p53 **(E)**, Tau **(F)**, β-actin **(G)**, and amyloid precursor protein (APP) **(H)** was quantified by digital imaging in arbitrary densitometry units (D.U.). In addition, APP **(I)** mRNA and 18S rRNA **(J)** levels were measured by real-time quantitative reverse-transcribed polymerase chain reaction (see Materials and Methods section). Graphs depict the group mean ± SEM results from 10 p-Luc control and 15 p-hNOS3-injected rats. Intergroup differences were compared using Student *t*-tests, and significant p values are indicated over the bars.

significantly reduced in the temporal lobes of p-hNOS3-inoculated brains relative to the p-Luc inoculated control brains (Fig. 3A, B). Real-time quantitative RT-PCR studies demonstrated significantly reduced expression of the Hu neuronal (Fig. 3C) and choline acetyltransferase (Fig. 3E) genes in p-hNOS3-inoculated relative to p-Luc-inoculated control brains. In contrast, there were no significant intergroup differences for myelin-associated glycoprotein-1 (Fig. 3D) or acetylcholinesterase (Fig. 3F) mRNA transcript levels.

Immunohistochemical staining studies demonstrated increased NOS3 immunoreactivity in vessel walls and parenchymal cells in the p-hNOS3-injected relative to control brains (Fig. 4A, B). In addition, the p-hNOS3-inoculated brains had increased immunoreactivity for GFAP (Fig. 4C, D), single-stranded DNA, reflecting increased DNA damage (Fig. 4E, F), Bax (proapoptosis; Fig. 4G, H), p53 (proapoptosis; Fig. 4I, J), and APP-Aβ (Fig. 4K, L). Importantly, p53, Bax, and single-stranded DNA immunoreactivities were localized in nuclei of various cell types within the cortex and white matter of p-hNOS3-injected brains, reflecting broadly increased proapoptosis gene expression and DNA damage with NOS3 overexpression. The increased GFAP immunoreactivity associated with NOS3 overexpression was distributed in the subpial, perivascular, and periventricular zones and within the neuropil and white matter parenchyma and may have reflected an earlier wave of neuronal loss as demonstrated by the reduced levels of Hu and lower mean cell densities detected by image analysis of the temporal lobes. Studies of brains harvested at earlier time periods suggest that the NOS3-mediated neuronal death occurred mainly within the first week after gene delivery (data not shown).

Effect of NOS3 Alzheimer Disease-Associated Proteins

Corresponding with the immunohistochemical staining results, Western blot analysis demonstrated increased levels of p53 protein expression in brains transfected with p-hNOS3 relative to p-Luc-transfected control brains (Fig. 5A). The Western blot signals were quantified by digital image densitometry. Student *t*-test analysis demonstrated significantly higher mean levels of p53 protein in the p-hNOS3-treansfected brains relative to control brains ($p = 0.005$) (Fig. 5E).

Tau protein was detected in all samples by Western blot analysis. However, in brains inoculated with p-hNOS3, the levels of Tau protein were increased, and the Western blot signals had a broad size range (~45–75 kDa) compared with the expected ~50-kDa band detected in control brains (Fig. 5B). Digital image analysis of the autoradiographs demonstrated significantly higher mean levels of Tau in brains transfected with p-hNOS3 relative to those inoculated with p-Luc ($p = 0.0008$) (Fig. 5F). The super-shifted bands (>50 kDa) were interpreted to represent phospho-Tau, and, correspondingly, additional studies demonstrated increased phospho-Tau immunoreactivity in the p-hNOS3-inoculated brains (Supplementary Fig. 1).

Studies were done to characterize the effects of NOS3 overexpression on APP expression. Western blot analysis demonstrated significantly increased levels of APP (Fig. 5C, H) ($p = 0.0009$) immunoreactivity in brains transfected with p-hNOS3 relative to those transfected with p-Luc. Correspondingly, real-time quantitative RT-PCR analyses demonstrated significantly higher levels of APP mRNA (Fig. 5I), and immunohistochemical staining demonstrated increased levels of APP-Aβ immunoreactivity (Fig. 4K, L) in the p-hNOS3-inoculated-brains relative to control brains. In contrast, β-actin protein (Fig. 5G) and 18S rRNA (Fig. 5J) levels were similar in the p-hNOS3-transfected and p-Luc-transfected brains.

To determine whether the NOS3 overexpression resulted in increased glycogen synthase kinase 3β (GSK-3β)

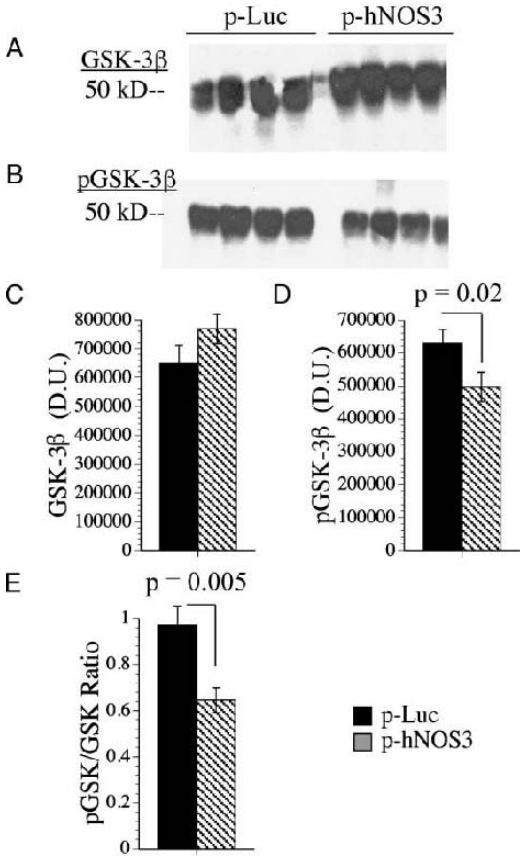

FIGURE 6. NOS3 overexpression increases glycogen synthase kinase 3β (GSK-3β) activity. Temporal cortex tissue was subjected to Western blot analysis to measure **(A)** total GSK-3β, and **(B)** phospho (p)-GSK-3β. Each lane in the representative blots shown corresponds to an individual rat brain. The position of the ~50 kDa molecular weight standard is shown at the left. Immunoreactivity was quantified by digital imaging in arbitrary densitometry units (D.U.), and the graphs depict the mean ± SEM levels of GSK-3β **(C)** and p-GSK-3β **(D)** and the calculated mean ± SEM ratios of p-GSK-3β and GSK-3β **(E)** in corresponding samples from 12 p-Luc control and 15 p-hNOS3-injected rats. Intergroup differences were evaluated using Student *t*-tests, and significant p values are indicated over the bars.

activity, the levels of phospho (p)-GSK-3β and total GSK-3β proteins were measured by Western blot analysis. Because p-GSK-3β is inactive, the ratio of p-GSK-3β to total GSK-3β provides an index of GSK-3β activity. Thus, a relatively low level of p-GSK-3β indicates increased GSK-3β activity, whereas a relatively high level of p-GSK-3β corresponds to reduced GSK-3β activity. Western blot analysis demonstrated only slightly higher levels of total GSK-3β (Fig. 6A, C) but significantly reduced levels of p-GSK-3β (Fig. 6B, D) ($p = 0.02$) in the p-hNOS3-transfected brains relative to control brains. In addition, the mean calculated ratio of p-GSK-3β/total GSK-3β was significantly reduced, reflecting higher GSK-3β activity in the p-hNOS3-transfected brains relative to the p-Luc-transfected control brains (Fig. 6E) ($p = 0.005$).

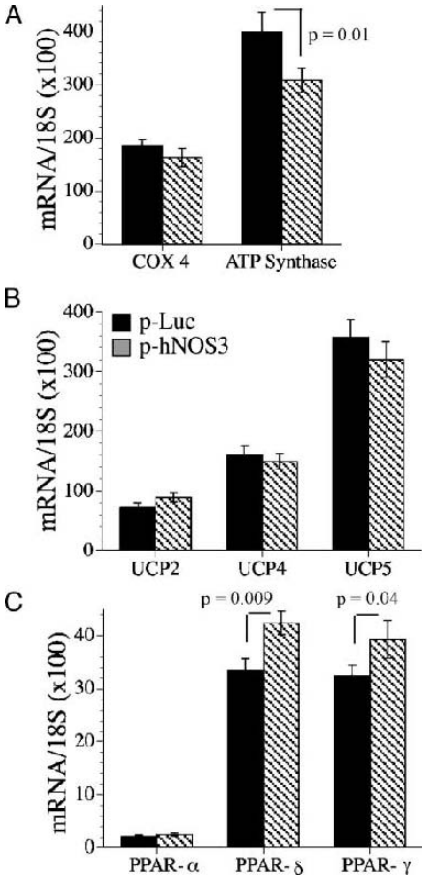

FIGURE 7. NOS3-induced changes in the expression of mitochondria-associated genes. The mRNA levels of cytochrome oxidase, subunit 4 (COX 4) and ATP synthase **(A)**, uncoupling proteins (UCP) 2, 4, and 5 **(B)**, and peroxisome proliferator-activated receptor (PPAR) subtypes α, δ, and γ **(C)** were measured in temporal lobe tissue harvested 30 days after p-Luc (n = 8) or p-hNOS3 (n = 12) gene delivery. Gene expression was measured by real-time quantitative reverse-transcribed polymerase chain reaction with results normalized to 18S rRNA (see Materials and Methods section). Graphs depict the mean ± SEM levels of gene expression. Intergroup differences were evaluated using Student *t*-tests, and significant p values are indicated over the bars.

Effects of NOS3 Overexpression on Genes Associated With Neuronal Survival and Neuroprotection

Real-time quantitative RT-PCR analysis was used to measure mRNA levels of mitochondria-encoded COX, ATP synthase (subunit 5), UCP2, UCP4, and UCP5, and nuclear-encoded PPAR-α, PPAR-δ, and PPAR-γ because these genes, along with NOS3, were demonstrated to be aberrantly expressed in AD (42). The studies demonstrated significantly reduced mean levels of ATP synthase (Fig. 7A) ($p = 0.008$) in the p-hNOS3-transfected brains relative to control brains. In contrast, the mean levels of COX mRNA were similar for the two groups (Fig. 7A). The three isoforms of UCP were differentially expressed in the brain such that UCP2 was the least abundant, UCP4 was intermediate, and UCP5 was the most abundant of the mRNA transcripts (Fig. 7B). Intergroup comparisons demonstrated no significant differences in the mean levels of UCP2, UCP4, or UCP5 between the p-hNOS3- and p-Luc-transfected brains. Studies of PPAR mRNA revealed very low levels of PPAR-α, and relatively high levels of both PPAR-δ and PPAR-γ in the cerebral cortex. Intergroup comparisons demonstrated significantly increased mean levels of PPAR-δ ($p = 0.009$) and PPAR-γ ($p = 0.04$) in the p-hNOS3-transfected brains relative to the p-Luc-inoculated control brains (Fig. 7C).

DISCUSSION

In AD, NOS3 expression is strikingly increased in corticolimbic structures, which represent major targets of neurodegeneration (31–33). In Down syndrome, abnormally increased NOS3 expression begins early in the course of AD-type neurodegeneration (31–33). The concept that NOS3 may also have a pivotal role in other aging-associated human neurodegenerative diseases was suggested by the finding of increased NOS3 expression in brains with Parkinson disease, diffuse Lewy body disease, Pick disease, amyotrophic lateral sclerosis, and multiple system atrophy and principally within the structural targets of neurodegeneration (33). Importantly, the aberrantly increased levels of NOS3 overlapped with the distributions of increased p53 and Fas (32, 33, 43), which are proapoptotic, and with nitrotyrosine, a marker of peroxynitrite (33) that causes oxidative injury, mitochondrial dysfunction, and neuronal death (35).

In the present study, we used a novel gene transfer model to examine the effects of NOS3 overexpression in vivo, and determined the extent to which AD and other neurodegenerative disease-associated neuropathologic and molecular abnormalities were caused by increased NOS3 expression. Quantitative real-time RT-PCR and Western blot assays confirmed the increased levels of human NOS3 in the rat brains and persistent expression of the transgene for up to 30 days. The prolonged period of foreign gene expression observed is reminiscent of results obtained by intramuscular injection of plasmid DNA for DNA-based immunization (44–46), suggesting that postmitotic cells can retain and express recombinant plasmid DNA for long intervals after transfection. Therefore, this model permits the study of short- and long-term effects of overexpressing or depleting

specific genes in the otherwise normal brain. The degree to which NOS3 expression was increased relative to control was similar to findings in AD and other neurodegenerative diseases (31,33). However, individual variation was attributed to variability in transfection efficiency.

The molecular and immunohistochemical staining studies demonstrated that constitutive overexpression of NOS3 in the brain caused neuronal loss with gliosis, associated with increased indices of DNA damage and the propensity for apoptosis, as occur in AD and other types of neurodegeneration (21, 22, 28, 29, 47, 48). These findings correspond with previous observations demonstrating that NOS3 overexpression (35) or oxidative injury itself (35, 49–56) causes DNA damage, mitochondrial dysfunction, and proapoptosis gene activation in neurons and support the hypothesis that enhanced NOS3 expression mediates neuronal loss in AD (32, 33, 43). Alternatively, the effects of increased NOS3 expression on neuronal death may be indirect and caused by increased p53- and Bax-mediated proneness for apoptosis as previously suggested for AD (27).

In brains inoculated with p-hNOS3, the increased levels of Tau with no alterations in β-actin suggest that Tau may selectively accumulate in brains with NOS3 overexpression. In addition, the increased levels of phospho-Tau could be explained by both increased Tau accumulation and increased GSK-3β activity. In AD, increased Tau phosphorylation is due to activation of proline-directed kinases including mitogen-activated protein kinases, cyclin-dependent kinase-5, and GSK-3β (57, 58), but Tau phosphorylation is also increased by oxidative stress activation of GSK-3β (59,60). Therefore, the increased Tau and phospho-Tau in p-hNOS3 inoculated brains may reflect responses to NOS3-induced oxidative stress.

The increased APP gene expression in p-hNOS3-inoculated brains corresponds with recent findings in sporadic AD (40, 41) and established findings in Down syndrome (61). In sporadic AD, increased APP-Aβ immunoreactivity is associated with upregulation of both the NOS3 and APP genes (40, 41). In Down syndrome, APP is overexpressed due to an extra copy of the Down syndrome locus, and NOS3 gene upregulation coincides with progressive accumulation of APP-Aβ in the brain (61). Moreover, previous in vitro studies showed that overexpression of NOS3 causes APP gene upregulation and increased APP-Aβ immunoreactivity (35), as observed in the p-hNOS3 inoculated brains. Together, these observations suggest that NOS3 and APP overexpressions are linked in human disease and experimental models and that constitutively increased expression of APP is sufficient to promote APP-Aβ accumulation, with no requirement for mutation of the APP gene or its regulatory/modifying genes (62–64). The mechanisms underlying this effect again may be increased oxidative stress, which promotes APP cleavage and generation of APP-Aβ immunoreactive C-terminal fragments (65, 66).

In AD, neuronal loss in the brain is correlated with DNA damage, mitochondrial dysfunction, and reduced mitochondrial gene expression (23, 67, 68). In vitro studies also showed that NOS activation or upregulated gene expression impairs mitochondrial gene expression and function due to increased mitochondrial DNA damage, intracellular accumulation of reactive oxygen species, and stimulation of proapoptosis mechanisms (35, 69–71). To determine whether the same phenomena occur in vivo and whether compensatory mechanisms are activated in response to mitochondrial dysfunction, mRNA levels of COX4, ATP synthase, UCP, and PPAR were measured. The results demonstrated that ATP synthase expression was significantly reduced in the p-hNOS3-transfected brains, consistent with a previous report demonstrating NO-mediated inhibition of ATP synthase (70). Because ATP synthase (Complex V) catalyzes the synthesis of ATP from ADP and Pi in the mitochondria, reduced levels of ATP synthase expression could lead to insufficient energy required for functions such as glucose transport and maintenance of cell membrane integrity.

UCPs dissipate the electrochemical gradient and allow electron transport while inhibiting ATP synthesis and are increased in response to oxidative stress. In this regard, recent studies demonstrated a neuroprotective role for UCP2 in relation to oxidative injury (72). In neuronal cells, brain-specific UCP4 and UCP5 have a more dominant role than UCP2 for protecting against oxidative stress (73), and, therefore, we expected that UCP4 and UCP5 expression levels would be up-regulated in response to increased levels of NOS3 in the brain. However, this was not the case as no significant differences in the mean mRNA levels of UCP2, UCP4, or UCP5 were detected between the p-hNOS3- and p-Luc-transfected brains. One potential explanation for this result is that ATP synthase expression was already reduced and therefore, uncoupling of oxidative phosphorylation might not have been a beneficial response for cells in an energy-deficient state.

PPARs have important roles in protecting cells from the adverse effects of lipid peroxidation (74–76). Lipid peroxidation is a recognized consequence of oxidative stress, and consequently, lipid peroxidation products are increased in brains with AD or other neurodegenerative diseases (77–79), as well as in experimental NOS-induced mitochondrial dysfunction and oxidative stress (9). The studies herein demonstrated that PPAR-δ and PPAR-γ were more abundantly expressed than PPAR-α and that the mean levels of both PPAR-δ and PPAR-γ were significantly higher in brains inoculated with p-hNOS3 than with p-Luc. These results suggest that chronically increased levels of NOS3 and oxidative stress can drive compensatory increases in PPAR gene expression, possibly as a cytoprotective response. It is tempting to speculate that treatment with the appropriate ligands may further improve the viability and function of neuronal cells at risk for NOS3-mediated neurodegeneration, as recently suggested (80, 81) and as demonstrated experimentally through the therapeutic use of PPAR agonists (82, 83), including use in another model of AD-type neurodegeneration (84).

The aggregate findings suggest that NOS3 overexpression in the brain causes tissue injury, gliosis, activation of proapoptotic mechanisms, and molecular abnormalities linked to AD-type neurodegeneration including reduced levels of mitochondrial gene expression and increased levels of phospho-Tau, APP, APP-Aβ, and GSK-3β activity. It

should be emphasized that the phenotype produced by overexpression of NOS3 was not identical to that for AD. In particular, there were no neurofibrillary tangles or neuritic plaques. The dissimilarities between the NOS3 model and AD were expected because of major differences in the time course of altered gene expression and the method used to upregulate the NOS3 gene. Nonetheless, the findings demonstrate that overexpression of NOS3 can reproduce several of the molecular abnormalities associated with AD.

REFERENCES

1. Schmidt H, Walter U. NO at work. Cell 1994;78:919–25
2. Koch K, Lambrecht H, Haberecht M, et al. Functional coupling of a Ca^{2+}/calmodulin dependent nitric oxide synthase and a soluble guanylyl cyclase in vertebrate photoreceptor cells. EMBO J 1994;13:3312–20
3. Lincoln J, Hoyle CHV, Burnstock G. *Nitric Oxide in Health and Disease*, 1st ed. Cambridge, UK: Cambridge University Press, 1997
4. Klatt P, Heinzel B, John M, et al. Ca^{2+}/calmodulin-dependent cytochrome *c* reductase activity of brain nitric oxide synthase. J Biol Chem 1992;267:11374–78
5. Boje K, Arora P. Microglial-produced nitric oxide and reactive nitrogen oxides mediate neuronal cell death. Brain Res 1992;587:250–56
6. Koprowski H, Zheng Y, Heber-Katz E, et al. In vivo expression of inducible nitric oxide synthase in experimentally induced neurologic diseases. Proc Natl Acad Sci USA 1993;90:3024–27
7. Merrill J, Ignarro L, Sherman M, et al. Microglial cell cytotoxicity of oligodendrocytes is mediated through nitric oxide. J Immunol 1993; 151:2132–41
8. Ghafourifar P, Richter C. Nitric oxide synthase activity in mitochondria. FEBS Lett 1997;418:291–96
9. Ghafourifar P, Schenk U, Klein SD, et al. Mitochondrial nitric-oxide synthase stimulation causes cytochrome *c* release from isolated mitochondria: evidence for intramitochondrial peroxynitrite formation. J Biol Chem 1999;274:31185–88
10. Giulivi C, Poderoso JJ, Boveris A. Production of nitric oxide by mitochondria. J Biol Chem 1998;273:11038–43
11. Hess D, Patterson S, Smith D, et al. Neuronal growth cone collapse and inhibition of protein fatty acylation by nitric oxide. Nature 1994;366: 562–65
12. Mesenge C, Verrecchia C, Allix M, et al. Reduction of the neurological deficit in mice with traumatic brain injury by nitric oxide synthase inhibitors. J Neurotrauma 1996;13:11–16
13. Klatt P, Schmidt K, Uray G, et al. Multiple catalytic functions of brain nitric oxide synthase: Biochemical characterization, cofactor requirement, and the role of Nw-hydroxy-l-arginine as an intermediate. J Biol Chem 1993;268:14781–87
14. Nishikawa T, Kirsch J, Koehler R, et al. Effect of nitric oxide synthase inhibition on cerebral blood flow and injury volume during focal ischemia in cats. Stroke 1993;24:1717–24
15. Satou T, Cummings BJ, Cotman CW, et al. Immunoreactivity for Bcl-2 protein within neurons in the Alzheimer's disease brain increases with disease severity. Brain Res 1995;697:35–43
16. Bredt D, Snyder S. Transient nitric oxide synthase neurons in embryonic cerebral cortical plate, sensory ganglia, and olfactory epithelium. Neuron 1994;13:301–13
17. Dinerman JL, Dawson TM, Schell MJ, et al. Endothelial nitric oxide synthase localized to hippocampal pyramidal cells: Implications for synaptic plasticity. Proc Natl Acad Sci USA 1994;91:4214–18
18. O'Dell TJ, Huang PL, Dawson TM, et al. Endothelial NOS and the blockade of LTP by NOS inhibitors in mice lacking neuronal NOS. Science 1994;265:542–46
19. Esiri M, Morris JE. *The Neuropathology of Dementia*. Cambridge, UK: Cambridge University Press, 1997
20. Cotman CW, Su JH. Mechanisms of neuronal death in Alzheimer's disease. Brain Pathol 1996;6:493–506
21. de la Monte SM, Sohn YK, Wands JR. Correlates of p53- and Fas (CD95)-mediated apoptosis in Alzheimer's disease. J Neurol Sci 1997; 152:73–83
22. de la Monte SM, Sohn YK, Ganju N, et al. P53- and CD95-associated apoptosis in neurodegenerative diseases. Lab Invest 1998;78:401–11
23. de la Monte SM, Luong T, Neely TR, et al. Mitochondrial DNA damage as a mechanism of cell loss in Alzheimer's disease. Lab Invest 2000;80:1323–35
24. Kitamura Y, Shimohama S, Kamoshima W, et al. Alteration of proteins regulating apoptosis, Bcl-2, Bcl-x, Bax, Bak, Bad, ICH-1 and CPP32, in Alzheimer's disease. Brain Res 1998;780:260–69
25. MacGibbon GA, Lawlor PA, Sirimanne ES, et al. Bax expression in mammalian neurons undergoing apoptosis, and in Alzheimer's disease hippocampus. Brain Res 1997;750:223–34
26. Perry G, Nunomura A. Apoptosis and Alzheimer's disease (Letter). Science 1998;282:1268–69
27. Stadelmann C, Bruck W, Bancher C, et al. Alzheimer disease: DNA fragmentation indicates increased neuronal vulnerability, but not apoptosis. J Neuropathol Exp Neurol 1998;57:456–64
28. Su JH, Anderson AJ, Cummings BJ, Cotman CW. Immunohistochemical evidence for apoptosis in Alzheimer's disease. Neuroreport 1994;5: 2529–33
29. Su JH, Deng G, Cotman CW. Bax protein expression is increased in Alzheimer's brain: correlations with DNA damage, Bcl-2 expression, and brain pathology. J Neuropathol Exp Neurol 1997;56:86–93
30. Tortosa A, Lopez E, Ferrer I. Bcl-2 and Bax protein expression in Alzheimer's disease. Acta Neuropathol (Berl) 1998;95:407–12
31. de la Monte S, Bloch K. Aberrant expression of the constitutive endothelial nitric oxide synthase gene in Alzheimer's disease. Mol Chem Neuropathol 1997;30:139–59
32. de la Monte SM, Lu BX, Sohn YK, et al. Aberrant expression of nitric oxide synthase III in Alzheimer's disease: Relevance to cerebral vasculopathy and neurodegeneration. Neurobiol Aging 2000;21:309–19
33. Sohn YK, Ganju N, Bloch KD, et al. Neuritic sprouting with aberrant expression of the nitric oxide synthase III gene in neurodegenerative diseases. J Neurol Sci 1999;162:133–51
34. Vodovotz Y, Lucia M, Flanders K, et al. Inducible nitric oxide synthase in tangle-bearing neurons of patients with Alzheimer's disease. J Exp Med 1996;184:1425–33
35. de la Monte SM, Chiche J, von dem Bussche A, et al. Nitric oxide synthase-3 overexpression causes apoptosis and impairs neuronal mitochondrial function: Relevance to Alzheimer's-type neurodegeneration. Lab Invest 2003;83:287–98
36. Xu J, Yeon JE, Chang H, et al. Ethanol impairs insulin-stimulated neuronal survival in the developing brain: Role of PTEN phosphatase. J Biol Chem 2003;278:26929–37
37. Yeon JE, Califano S, Xu J. Potential role of PTEN phosphatase in ethanol-impaired survival signaling in the liver. Hepatology 2003;38: 703–14
38. Ausubel F, Brent R, Kingston R, et al. *Current Protocols in Molecular Biology.* New York, NY: Wiley Interscience, 2000
39. Lester-Coll N, Rivera EJ, Soscia SJ. Intracerebral streptozotocin model of type 3 diabetes: Relevance to sporadic Alzheimer's disease. J Alzheimers Dis 2006;9:13–33
40. Rivera EJ, Goldin A, Fulmer N, et al. Insulin and insulin-like growth factor expression and function deteriorate with progression of Alzheimer's disease: Link to brain reductions in acetylcholine. J Alzheimers Dis 2005;8:247–68
41. Steen E, Terry BM, Rivera EJ, et al. Impaired insulin and insulin-like growth factor expression and signaling mechanisms in Alzheimer's disease-is this type 3 diabetes? J Alzheimers Dis 2005;7:63–80
42. de la Monte SM, Wands JR. Molecular indices of oxidative stress and mitochondrial dysfunction occur early and often progress with severity of Alzheimer's disease. J Alzheimers Dis 2006;9:167–81
43. de la Monte SM, Sohn YK, Etienne D, et al. Role of aberrant nitric oxide synthase-3 expression in cerebrovascular degeneration and vascular-mediated injury in Alzheimer's disease. Ann NY Acad Sci 2000;903:61–71
44. Mir LM, Bureau MF, Rangara R, et al. Long-term, high level in vivo gene expression after electric pulse-mediated gene transfer into skeletal muscle. CR Acad Sci III 1998;321:893–99
45. Maruyama H, Ataka K, Gejyo F, et al. Long-term production of erythropoietin after electroporation-mediated transfer of plasmid DNA into the muscles of normal and uremic rats. Gene Ther 2001; 8:461–68

46. Draghia-Akli R, Ellis KM, Hill LA, et al. High-efficiency growth hormone-releasing hormone plasmid vector administration into skeletal muscle mediated by electroporation in pigs. FASEB J 2003;17:526–28
47. Nagy ZS, Esiri MM. Apoptosis-related protein expression in the hippocampus in Alzheimer's disease. Neurobiol Aging 1997;18: 565–71
48. Anderson AJ, Su JH, Cotman CW. DNA damage and apoptosis in Alzheimer's disease: Colocalization with c-Jun immunoreactivity, relationship to brain area, and effect of postmortem delay. J Neurosci 1996;16:1710–19
49. Jacotot E, Costantini P, Laboureau E, et al. Mitochondrial membrane permeabilization during the apoptotic process. Ann NY Acad Sci 1999; 887:18–30
50. Bosca L, Hortelano S. Mechanisms of nitric oxide-dependent apoptosis: Involvement of mitochondrial mediators. Cell Signal 1999;11239–44
51. de la Monte SM, Neely TR, Cannon J, et al. Oxidative stress and hypoxia-like injury cause Alzheimer-type molecular abnormalities in central nervous system neurons. Cell Mol Life Sci 2000;57:1471–81
52. Lemasters JJ, Qian T, He L, et al. Role of mitochondrial inner membrane permeabilization in necrotic cell death, apoptosis, and autophagy. Antioxid Redox Signal 2002;4:769–81
53. Yakes FM, Van Houten B. Mitochondrial DNA damage is more extensive and persists longer than nuclear DNA damage in human cells following oxidative stress. Proc Natl Acad Sci USA 1997;94:514–19
54. Budd SL, Tenneti L, Lishnak T, et al. Mitochondrial and extramitochondrial apoptotic signaling pathways in cerebrocortical neurons. Proc Natl Acad Sci USA 2000;97:6161–66
55. Korsmeyer SJ, Shutter JR, Veis DJ, et al. Bcl-2/Bax: A rheostat that regulates an anti-oxidant pathway and cell death. Semin Cancer Biol 1993;4:327–32
56. Crawford DR, Lauzon RJ, Wang Y, et al. 16S mitochondrial ribosomal RNA degradation is associated with apoptosis. Free Radic Biol Med 1997;22:1295–1300
57. Jackson GR, Wiedau-Pazos M, Sang TK, et al. Human wild-type tau interacts with wingless pathway components and produces neurofibrillary pathology in *Drosophila*. Neuron 2002;34:509–19
58. Veeranna GJ, Shetty KT, Takahashi M, et al. Cdk5 and MAPK are associated with complexes of cytoskeletal proteins in rat brain. Brain Res Mol Brain Res 2000;76:229–36
59. Crowder RJ, Freeman RS. Glycogen synthase kinase-3 β activity is critical for neuronal death caused by inhibiting phosphatidylinositol 3-kinase or Akt but not for death caused by nerve growth factor withdrawal. J Biol Chem 2000;275:34266–71
60. Hetman M, Cavanaugh JE, Kimelman D, et al. Role of glycogen synthase kinase-3β in neuronal apoptosis induced by trophic withdrawal. J Neurosci 2000;20:2567–74
61. de la Monte SM. Molecular abnormalities of the brain in Down syndrome: Relevance to Alzheimer's neurodegeneration. J Neural Transm 1999;57(Suppl):1–19
62. Tandon A, Frasier P. The presenilins. Genome Biol 2002;3:reviews3014
63. Sambamurti K, Greig NH, Lahiri DK. Advances in the cellular and molecular biology of the β-amyloid protein in Alzheimer's disease. Neuromolecular Med 2002;1:1–31
64. Rogaeva E. The solved and unsolved mysteries of the genetics of early-onset Alzheimer's disease. Neuromolecular Med 2002;2:1–10
65. Badan I, Platt D, Kessler C, et al. Temporal dynamics of degenerative and regenerative events associated with cerebral ischemia in aged rats. Gerontology 2003;49:356–65
66. Chen GJ, Xu J, Lahousse SA, et al. Transient hypoxia causes Alzheimer-type molecular and biochemical abnormalities in cortical neurons: Potential strategies for neuroprotection. J Alzheimers Dis 2003;5:209–28
67. Mattson MP, Pedersen WA, Duan W, et al. Cellular and molecular mechanisms underlying perturbed energy metabolism and neuronal degeneration in Alzheimer's and Parkinson's diseases. Ann NY Acad Sci 1999;893:154–75
68. Cassarino DS, Bennett JP Jr. An evaluation of the role of mitochondria in neurodegenerative diseases: Mitochondrial mutations and oxidative pathology, protective nuclear responses, and cell death in neurodegeneration. Brain Res Brain Res Rev 1999;29:1–25
69. Torok NJ, Higuchi H, Bronk S, et al. Nitric oxide inhibits apoptosis downstream of cytochrome C release by nitrosylating caspase 9. Cancer Res 2002;62:1648–53
70. Almeida A, Bolanos JP. A transient inhibition of mitochondrial ATP synthesis by nitric oxide synthase activation triggered apoptosis in primary cortical neurons. J Neurochem 2001;77:676–90
71. Ghafourifar P, Bringold U, Klein SD, et al. Mitochondrial nitric oxide synthase, oxidative stress and apoptosis. Biol Signals Recept 2001;10: 57–65
72. Horvath TL, Diano S, Barnstable C. Mitochondrial uncoupling protein 2 in the central nervous system: Neuromodulator and neuroprotector. Biochem Pharmacol 2003;65:1917–21
73. Mattson MP, Liu D. Mitochondrial potassium channels and uncoupling proteins in synaptic plasticity and neuronal cell death. Biochem Biophys Res Commun 2003;304:539–49
74. Bishop-Bailey D, Wray J. Peroxisome proliferator-activated receptors: A critical review on endogenous pathways for ligand generation. Prostaglandins Other Lipid Mediat 2003;71:1–22
75. Gilde AJ, Van Bilsen M. Peroxisome proliferator-activated receptors (PPARS): Regulators of gene expression in heart and skeletal muscle. Acta Physiol Scand 2003;178:425–34
76. Lee CH, Olson P, Evans RM. Minireview: Lipid metabolism, metabolic diseases, and peroxisome proliferator-activated receptors. Endocrinology 2003;144:2201–7
77. Sayre LM, Zelasko DA, Harris PL, et al. 4-Hydroxynonenal-derived advanced lipid peroxidation end products are increased in Alzheimer's disease. J Neurochem 1997;68:2092–97
78. Montine KS, Kim PJ, Olson SJ, et al. 4-Hydroxy-2-nonenal pyrrole adducts in human neurodegenerative disease. J Neuropathol Exp Neurol 1997;56:866–71
79. Markesbery WR, Carney JM. Oxidative alterations in Alzheimer's disease. Brain Pathol 1999;9:133–46
80. de la Monte SM, Wands JR. Alzheimer-associated neuronal thread protein mediated cell death is linked to impaired insulin signaling. J Alzheimers Dis 2003;6:231–42
81. Watson GS, Craft S. The role of insulin resistance in the pathogenesis of Alzheimer's disease: Implications for treatment. CNS Drugs 2003; 17:27–45
82. Deplanque D, Gele P, Petrault O, et al. Peroxisome proliferator-activated receptor-α activation as a mechanism of preventive neuroprotection induced by chronic fenofibrate treatment. J Neurosci 2003;23:6264–71
83. Sivarajah A, Chatterjee PK, Patel NS, et al. Agonists of peroxisome-proliferator activated receptor-γ reduce renal ischemia/reperfusion injury. Am J Nephrol 2003;23:267–76
84. de la Monte SM, Tong M, Lester-Coll N, et al. Therapeutic rescue of neurodegeneration in experimental type 3 diabetes: Relevance to Alzheimer's disease. J Alzheimers Dis 2006;10:89–109

